Bridging the gap between seismically and geodetically detected slow earthquakes

Satoshi Ide,[1] Kazutoshi Imanishi,[2] Yasuhiro Yoshida,[3] Gregory C. Beroza,[4] and David R. Shelly[5]

Received 16 March 2008; revised 7 April 2008; accepted 11 April 2008; published 22 May 2008.

[1] Recently observed unusual seismic events: deep low frequency earthquakes and tremor, very low frequency earthquakes, and slow slip events form a family of slow earthquakes that are governed by a scaling law different from ordinary earthquakes. Guided by this scaling law, we have observed previously unknown events, with source duration of 20–200 s and moment magnitude of 3–4, under the Kii Peninsula in western Japan. These events radiate seismic energy in the 2–8 Hz band in direct proportion to their seismic moment-rate, though the constant of proportionality is 4–5 orders of magnitude smaller than for ordinary earthquakes. Slow earthquakes in this region may be comprised of numerous shear slip events, which in aggregate are manifest seismically as tremor or isolated longer events up to 200 s and geodetically as slow slip events. **Citation:** Ide, S., K. Imanishi, Y. Yoshida, G. C. Beroza, and D. R. Shelly (2008), Bridging the gap between seismically and geodetically detected slow earthquakes, *Geophys. Res. Lett.*, *35*, L10305, doi:10.1029/2008GL034014.

1. Introduction

[2] Slow earthquakes are unusual earthquakes, recently discovered worldwide in subduction zones and the San Andreas Fault system in California [e.g., *Ide et al.*, 2007a; *Schwartz and Rokosky*, 2007]. In western Japan, slow earthquakes occur in a zone that follows the 35 km iso-depth contour of the top of the subducting Philippine Sea Plate, along the Nankai subduction zone. Slow earthquakes in this area are categorized into three groups based on their frequency/period ranges. Deep low frequency earthquakes and tremor [*Obara*, 2002; *Katsumata and Kamaya*, 2003], very low frequency earthquakes (VLF) [*Ito et al.*, 2007], and slow slip events (SSE) [e.g., *Hirose and Obara*, 2005] have been studied in the frequency/period range higher than 2 Hz, between 0.02–0.05 Hz, and longer than a few days, respectively. All these phenomena appear to be shear slip on the plate interface, and occur at the same time and place [*Shelly et al.*, 2006, 2007a; *Ide et al.*, 2007a, 2007b].

[3] *Ide et al.* [2007a] showed that slow earthquakes obey a simple scaling law, in which the seismic moment M_o is proportional to the duration T, as

$$M_0/T = 10^{12\text{-}13}\ (\mathrm{Nm/s}) \tag{1}$$

They also proposed that slow earthquakes grow from shear slip at a minimum size as small as moment magnitude (M_w) $\sim$ 1, which in isolation is observed as a deep low frequency earthquake. They predicted the existence of slow earthquakes with durations longer than VLFs. In this paper we report the detection of these hypothesized events and show that there is a characteristic constant that connects the static and dynamic sizes of each event.

2. A New Class of Slow Earthquakes

[4] Earthquakes radiate seismic waves most efficiently at periods longer than their characteristic duration. For this reason, the rapid increase of Earth noise with decreasing frequency [*Agnew and Berger*, 1978] makes detection of slow earthquakes increasingly difficult as the source duration increases. To find a long-period slow earthquake of about 100 s duration in seismograms, the noise amplitude at the frequencies of about 0.01 Hz must be quite low. This is satisfied only for the broadband vertical component of quiet seismographic stations. The number of useful stations is further limited because the long-period signal we seek is dominated by near-field terms that decay as the inverse of distance squared, and thus have a narrow amplitude peak near the epicenter. This contrasts with far-field waves that dominate at shorter periods and decay as the inverse of distance, and thus have much broader amplitude peaks. The F-net station KIS maintained by National Research Institute for Earth Science and Disaster Prevention (NIED), Japan satisfies these strict conditions (Figure 1).

[5] Streckeisen STS-1 broadband seismometers at KIS have recorded continuous data since March 1996. In this data, we can detect tremor lasting for 2–3 days, several times a year. Although the locations of the tremor sources are unknown for old data, the locations and timing of recent LFEs suggest that these signals persistently come from the region of tremor activity near the star symbol in Figure 1. Tremor is clearly visible in spectra of ground velocity as a period of increased, and almost constant, spectral amplitude in a broad frequency band between 0.01–10 Hz. Observations between 0.1–1 Hz are obscured by strong microseisms. Figure 2 shows an example of spectra and waveforms on September 29, 1999 (JST), when the signal to noise (S/N) ratio was particularly high. The waveforms are shown at three frequency ranges: 2–8, 0.05–0.02, and

[1]Department of Earth and Planetary Science, University of Tokyo, Tokyo, Japan.
[2]National Institute of Advanced Industrial Science and Technology, Tsukuba, Japan.
[3]Meteorological Research Institute, Tsukuba, Japan.
[4]Department of Geophysics, Stanford University, Stanford, California, USA.
[5]Department of Earth and Planetary Science, University of California, Berkeley, California, USA.

0094-8276/08/2008GL034014

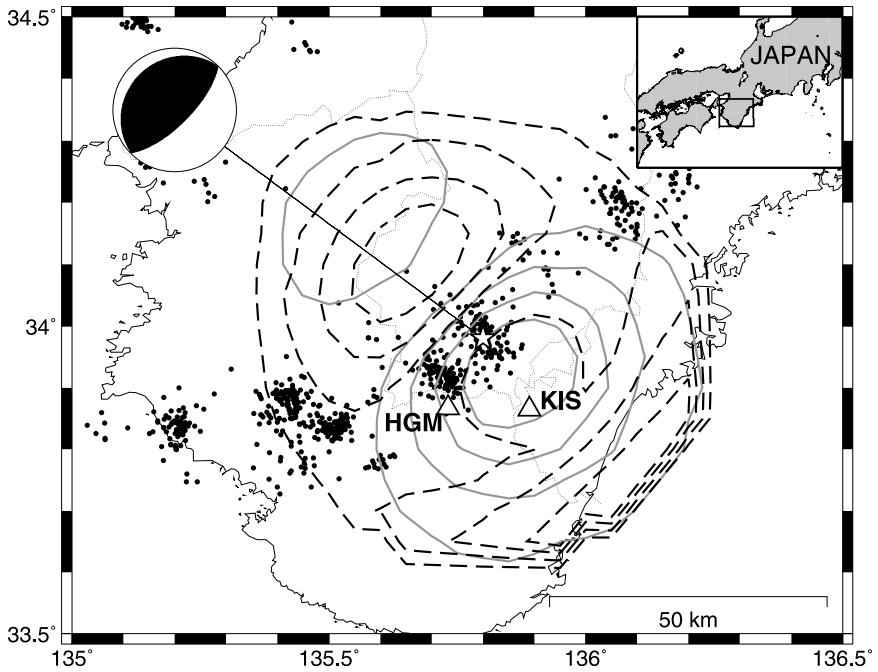

Figure 1. Map of the study area, Kii Peninsula, as shown in the upper right inset. Two triangles show the location of stations KIS and HGM. Black dots are the epicenters of LFEs determined by Japan Meteorological Agency. Gray bold lines are contours of the maximum amplitude of vertical ground velocity from a point source located at the star symbol at 35 km depth with the shown focal mechanism (beach ball) and a source duration of 100 s. Four contours show 20, 40, 60, and 80% of the maximum. Black dashed lines show the same quantity for a source of 1 s duration.

0.002–0.02 Hz. The first range is typically used to analyze deep tremor. VLFs were discovered in the middle range [*Ito et al.*, 2007]. We also observe waves of large amplitude in this range as shown in Figure 2. Therefore, it is possible to detect and locate many VLFs during this period. In some parts of the records, we observe even lower frequency waves (0.002–0.02 Hz) accompanying the tremor and VLF signals. Similar waves are observable during each of the tremor episodes that repeat at 3–6 month intervals. We extract about 200 time sections that include clear low frequency signals below 0.02 Hz with low noise from the 11-year continuous record of ground motion.

3. Moment Rate Function of a New Class of Slow Earthquakes

3.1. Method

[6] For each time section, we estimate a moment-rate function using the following method. The vertical seismic record is corrected for instrumental response, and bandpass filtered between 0.005–0.05 Hz. Assuming a point source location and a fault mechanism, we calculate the theoretical ground velocity from an impulsive moment-rate function using a layered structure. The moment-rate function at the source is expanded by 99 linear spline basis functions for 400 s around the maximum of the data. This function is convolved with the impulse response and compared with the data to determine the best-fit in the least square sense. We apply a non-negative constraint for the parameters, expansion coefficients of the moment-rate function, and also use prior information that the parameter values are almost zero. This problem is the point source version of the slip inversion method of *Ide and Takeo* [1997] and similarly solved by Bayesian modeling with the best estimates determined by Akaike's Bayesian Information Criterion [*Akaike*, 1980].

3.2. Results

[7] Figure 3a is an example from May 28, 2006, during which *Ito et al.* [2007] identified a VLF and determined its location and focal mechanism (strike 225°, dip 20°, and rake 90°). Although they reported a source duration of 20 s, the total duration is much longer. Assuming the same location and mechanism as the VLF, we determine that the moment-rate function has three peaks and a total duration of $\sim$ 100 s. Presumably, one of the peaks corresponds to the previously reported VLF. The seismic moment is 1.0×10^{15} Nm (M_w 4.0), which is over 5 times larger than the seismic moment of the M_w 3.5 VLF.

[8] Figure 3b shows another example, for which an additional record from a temporary Streckeisen STS-2 at station HGM, National Institute of Advanced Industrial Science and Technology, Japan, is also available. KIS and HGM are separated by 15 km (Figure 1) and record similar waveforms; however, the amplitudes of the waves are quite different even in the low-frequency range, as expected from the theoretical amplitude pattern of low-frequency waves (Figure 1). Since the S/N ratio of HGM is relatively low, we determine the moment-rate function using the record of KIS alone and calculate theoretical waves from this source to HGM. The location and focal mechanism are the same as in the previous case. This forward prediction explains the amplitude difference and the waveform similarity confirms that these low-frequency waves are consistent with a source with the assumed location and focal mechanism. The total duration is about 70 s.

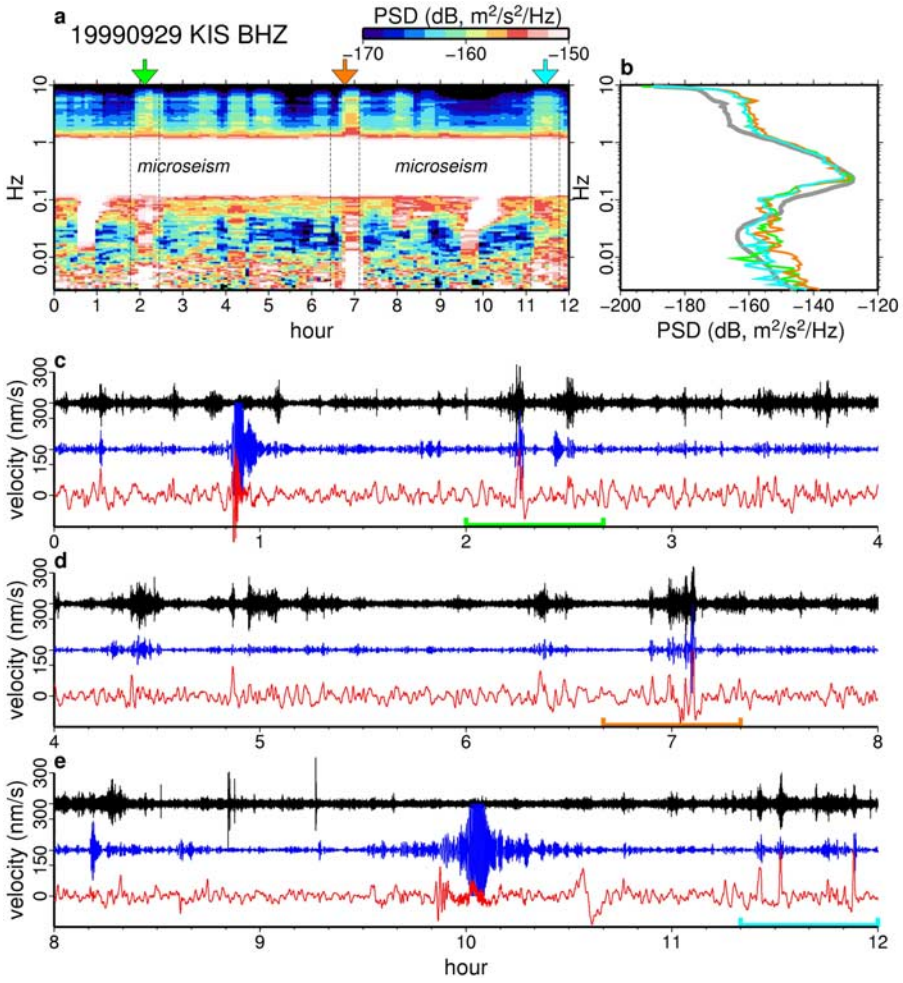

Figure 2. Examples of data recorded at station KIS. (a) A spectrogram of ground velocity on September 29, 1999 (JST). (b) Spectrum within three time windows shown in Figure 2a using corresponding colors. Gray line is yearly averaged spectrum at this station. (c–e) Waveforms in three different frequency ranges. Black, blue, and red lines are band-pass filtered ground velocity between 2–8, 0.02–0.05, and 0.002–0.02 Hz, respectively. Three active periods is identified as shown by arrows in Figure 2a and correspondingly colored lines in Figures 2b–2d.

[9] We determine moment-rate functions for all the selected events. Inevitably, the assumed source location and mechanism are not strictly correct. We assess the effect of errors in these parameters using a random simulation. The hypocentral parameters are re-sampled from Gaussian distribution with zero mean and standard deviation of 10 km. We also resample each of the three angles of the focal mechanism with standard deviation of 10°. We determine the moment-rate function using the resampled location and mechanism parameters. Although the shape of the function is little changed, the value of moment fluctuates somewhat. The distribution is almost log-normal, i.e., normal in moment magnitude with the standard deviation 0.17 in M_w.

3.3. Scaling Relations

[10] We calculate the source duration, maximum moment-rate, and seismic moment for each time section. The duration is measured as the continuous period for which the moment-rate is higher than 10% of the maximum (Figures 3a and 3b). The amplitudes of the moment-rate function are about 10^{13} Nm/s, which is consistent with the relation between seismic moment M_o and duration T in equation (1). Consequently, the duration and seismic moment estimated for all events falls within the predicted range (Figures 4a and 4b). A typical slow earthquake of about 100 s has moment magnitude of about 4. The best-fitting line to these data obeys a relationship of approximately $M_o \sim T^{1.5}$. This different scaling may be an artifact of the limited frequency range of our analysis, 0.005–0.05 Hz. The parameter errors are inherently large because of the uncertainty of seismic moment estimation and the difficulty of extracting durations from complex moment-rate functions. Artificially introduced upper and lower bounds will reshape the large scatter and introduce an artificial trend. Similar tendencies have been seen in scaling studies of earthquake parameters in different settings [e.g., *Ide and Beroza*, 2001].

4. Seismic Energy and Moment Release

[11] As shown in Figure 3c, the seismic moment-rate function determined in the low frequency range has a remarkably similar shape to the squared high-frequency velocity waveform. The squared velocity $\dot{u}^2$ is related to

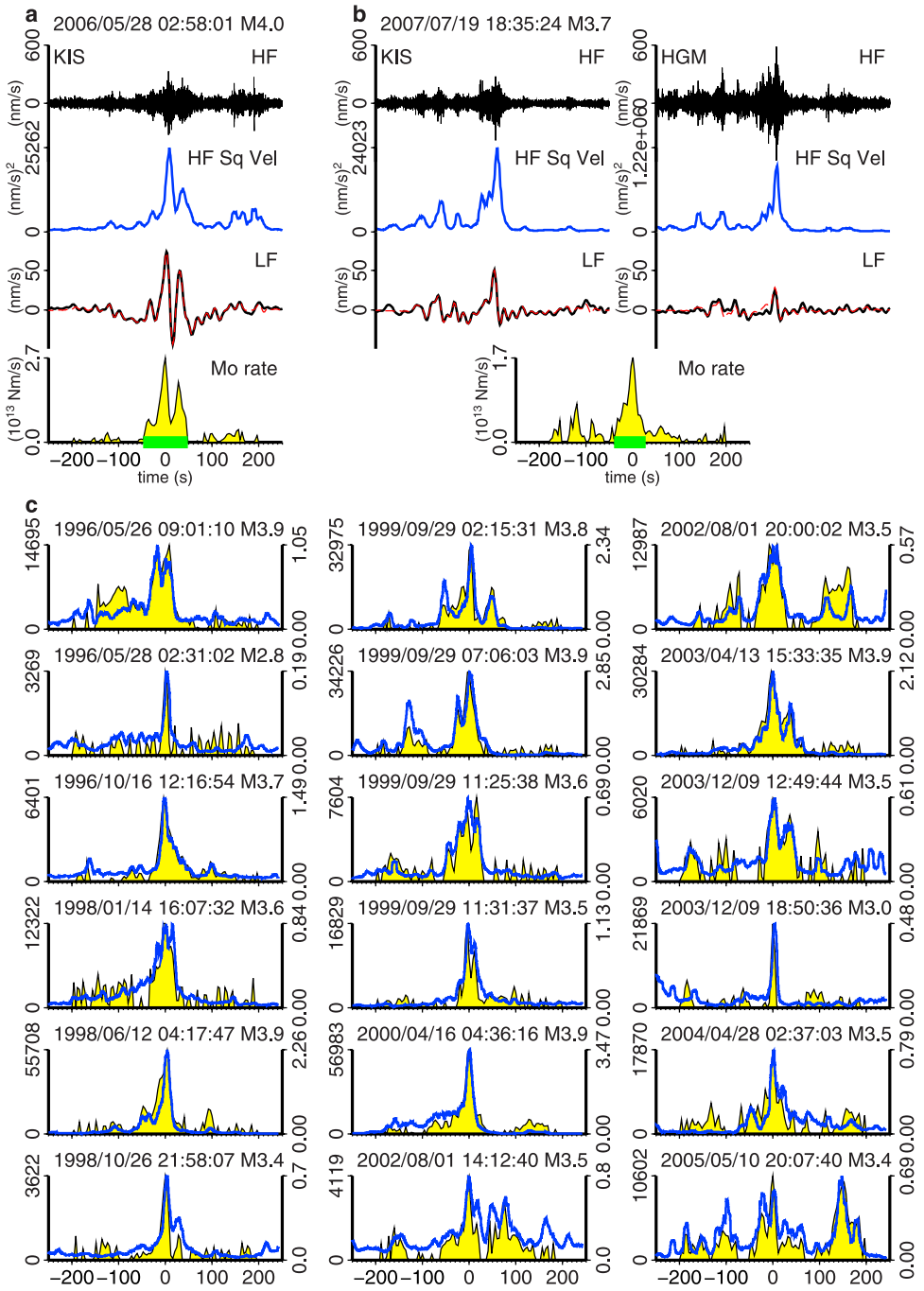

Figure 3. Estimated moment-rate functions. (a) Example for the event on May 28, 2006. "HF" and "LF" denote high-frequency and low-frequency waves between 2–8 and 0.005–0.05 Hz, respectively. "HF Sq Vel" denotes the squared velocity waveform, which is the summation of three component seismograms, filtered between 2–8 Hz and averaged using a 10 s boxcar window. "Mo rate" is the obtained moment-rate function, with an estimation of duration shown by the thick green line at the bottom. On the LF trace, synthetic waveforms calculated using the moment-rate function are shown by dashed red lines on the observed waveforms (black). (b) Example with data from two stations, on July 18, 2007. The moment-rate function is determined from KIS data alone, but calculated waves are shown for both stations. (c) Comparison between squared velocity seismograms (thick blue lines, left axis in nm^2/s^2) and moment-rate functions (yellow areas, right axis in 10^{13} Nm/s). The scale is different for each trace. The time of the former is advanced 8 s to account for the wave propagation time. Each event time is the time of local maximum of LF waves (JST). M indicates moment magnitude.

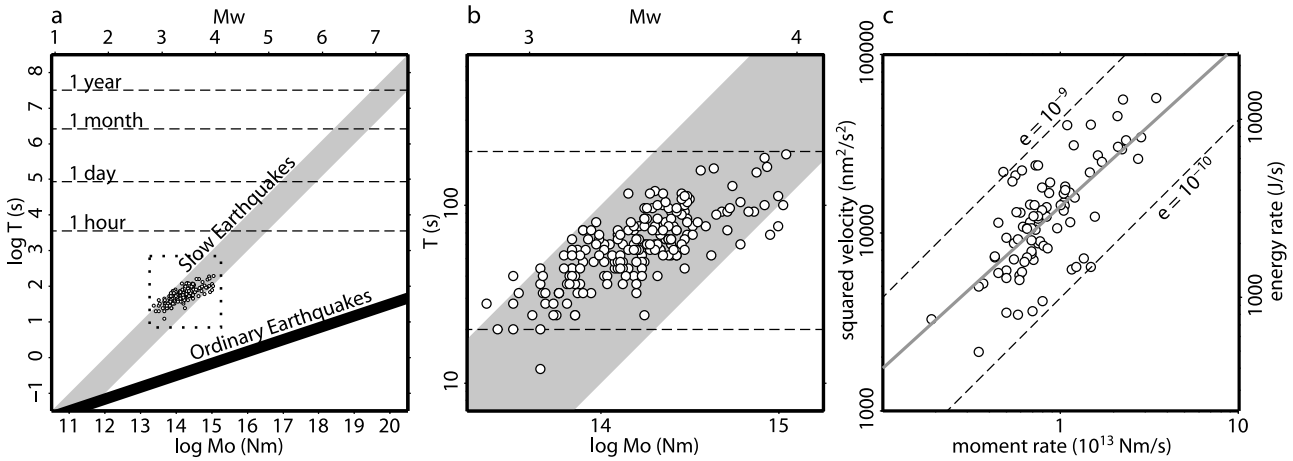

Figure 4. Scaling relations between source parameters. (a) Comparison between scaling laws for slow (gray zone) and ordinary earthquakes (black zone) presented by *Ide et al.* [2007a]. LFE, VLF, and SSE represent typical size and duration of these events. Dotted area is studied in the present study. (b) Gray zone shows the range of the scaling law for slow earthquakes. Dashed lines show approximate limitations due to limited frequency bandwidth. (c) The peak values of the moment-rate and radiated energy functions that are used to scale Figure 3c. Gray line is the least square fit, log10(squared velocity) = 0.91 log10 (moment-rate) + 4.14, in the units shown in the figure. Dashed lines show constant scaled energy e = 10^{-9} and 10^{-10}.

the radiated seismic energy in this range, neglecting small *P*-waves, as

$$\dot{E}_s \sim 4\pi r^2 \rho\beta \dot{u}^2 \sim 0.23 \times 10^{18} \dot{u}^2, \quad (2)$$

in SI units, where r, ρ, and β are the source-receiver distance, density, and *S*-wave velocity, respectively. The peak values of the moment-rate and radiated energy functions are proportional (Figure 4c), which means the ratio between seismic energy and seismic moment, known as the scaled energy [*Kanamori and Rivera*, 2006] is nearly constant. We find the scaled energy is between 10^{-10}–10^{-9}, which is dramatically smaller than ordinary earthquakes. Note that it is a lower bound due to the limited frequency range and that significant energy above this range may increase the scaled energy. The scaled energy of ordinary earthquakes are typically $\sim 3 \times 10^{-5}$ with perhaps a weak size-dependence over many orders of magnitudes in earthquake size [e.g., *Kanamori and Rivera*, 2006].

[12] There are instances during ordinary earthquakes for which the high frequency energy radiation and the seismic moment-rate function are considerably different, with large pulses of high-frequency seismic waves having little impact on the seismic moment history [*Sato et al.*, 1996; *Allmann and Shearer*, 2007]. The nearly identical shape of the radiated energy and moment-rate functions for the slow earthquakes we have studied is striking. One interpretation is that the slow slip responsible for the moment-rate function is setting off small, low frequency earthquakes that are detected as tremor energy. Another interpretation is that there is a short tremor unit with a characteristic seismic moment and seismic energy, that repeats many times, producing similar time functions for both energy radiation and seismic moment-rate. Both cases suggest that there is a unit process represented by the quantitative link between tremor energy and the amount of slow slip.

[13] We have applied equation (2) to slow earthquakes as long as 200 s duration, but it is interesting to consider whether or not it applies to SSEs that last much longer. No fault model for an SSE is available in the study area, so we compare tremor energy and SSE moment for the April, 2006 event in Shikoku, using data from 8 stations of NIED Hi-net for the period 4/15–4/21. We band-pass filtered each seismogram between 2–8 Hz, clipped the amplitude at 0.25 mm to minimize the contribution from nearby earthquakes We assumed a point source near the center of the dislocation model for this SSE. For the mean energy estimate we obtain 3.2×10^7 J and the seismic moment of corresponding SSE is 1.2×10^{18} Nm [*Sekine and Obara*, 2006]. Therefore, the scaled energy for this sequence is 2.7×10^{-11}. This is smaller by about an order of magnitude than the mean value obtained in this study (Figure 4c), but there are large uncertainties in the energy estimate and the moment of the SSE. The similarity of the two values suggests that the link between tremor energy and slow slip may hold for geodetically observed SSEs as well.

5. Discussion and Conclusion

[14] Our data, together with previous studies, suggests that the phenomena of LFEs, non-volcanic tremor, VLFs, and the 200 s slow earthquakes we report on in this paper, are all comprised of a unit process that may serve as the fundamental building block of each of these slow earthquakes. There are probably much longer, and larger events, with no clear upper limit up to the scale of SSE, but slow earthquakes that fall in the gap between 200 s and 1 day duration (Figure 4a) will be difficult to detect due to the increase in Earth noise in that period range. Recent studies have reported that deep tremor can be triggered by Earth tides [*Shelly et al.*, 2007b; *Rubinstein et al.*, 2007a] and

surface waves from distant large earthquakes [*Miyazawa and Mori*, 2005; *Rubinstein et al.*, 2007b]. Therefore, the characteristic period of these external effects might modulate slow earthquakes.

[15] The similarity between the moment-rate and energy-rate functions raises the possibility that there may be no purely aseismic motion in this area independent of tremor. If so, we can monitor and localize slow fault slip using tremor signals alone.

[16] **Acknowledgments.** This work is supported by Grant-in-Aid for Scientific Research, Ministry of Education, Sports, Science and Technology, Japan, and National Science Foundation grant EAR-0409917.

References

Agnew, D. C., and J. Berger (1978), Vertical seismic noise at very low frequencies, *J. Geophys. Res.*, *83*, 5420–5424.

Akaike, H. (1980), Likelihood and Bayes procedure, in *Bayesian Statistics*, edited by J. M. Bernardo et al., pp. 143–166, Univ. Press, Valencia, Spain.

Allmann, B. P., and P. M. Shearer (2007), A high-frequency secondary event during the 2004 Parkfield earthquake, *Science*, *318*, 1279–1283.

Hirose, H., and K. Obara (2005), Repeating short- and long-term slow slip events with deep tremor activity around the Bungo channel region, southwest Japan, *Earth Planets Space*, *57*, 961–972.

Ide, S., and G. C. Beroza (2001), Does apparent stress vary with earthquake size?, *Geophys. Res. Lett.*, *28*, 3349–3352.

Ide, S., and M. Takeo (1997), Determination of constitutive relations of fault slip based on seismic wave analysis, *J. Geophys. Res.*, *102*, 27,379–27,391.

Ide, S., G. C. Beroza, D. R. Shelly, and T. Uchide (2007a), A scaling law for slow earthquakes, *Nature*, *447*, 76–79.

Ide, S., D. R. Shelly, and G. C. Beroza (2007b), Mechanism of deep low frequency earthquakes: Further evidence that deep non-volcanic tremor is generated by shear slip on the plate interface, *Geophys. Res. Lett.*, *34*, L03308, doi:10.1029/2006GL028890.

Ito, Y., K. Obara, K. Shiomi, S. Sekine, and H. Hirose (2007), Slow earthquakes coincident with episodic tremors and slow slip events, *Science*, *315*, 503–506.

Kanamori, H., and L. Rivera (2006), Energy partitioning during an earthquake, in *Radiated Energy and the Physics of Earthquake Faulting*, *Geophys. Monogr. Ser.*, vol. 70, edited by R. Abercrombie et al., pp. 3–13, AGU, Washington, D.C.

Katsumata, A., and N. Kamaya (2003), Low-frequency continuous tremor around the Moho discontinuity away from volcanoes in the southwest Japan, *Geophys. Res. Lett.*, *30*(1), 1020, doi:10.1029/2002GL015981.

Miyazawa, M., and J. Mori (2005), Detection of triggered deep low-frequency events from the 2003 Tokachi-oki earthquake, *Geophys. Res. Lett.*, *32*, L10307, doi:10.1029/2005GL022539.

Obara, K. (2002), Nonvolcanic deep tremor associated with subduction in southwest Japan, *Science*, *296*, 1679–1681.

Rubinstein, J. L., M. L. Rocca, J. E. Vidale, K. C. Creager, and A. G. Wech (2007a), Tidal modulation of nonvolcanic tremor, *Science*, *319*, 186–189.

Rubinstein, J. L., J. E. Vidale, J. Gomberg, P. Bodin, K. C. Creager, and S. D. Malone (2007b), Non-volcanic tremor driven by large transient shear stresses, *Nature*, *448*, 579–582.

Sato, T., K. Imanishi, and M. Kosuga (1996), Three-stage rupture process of the 28 December 1994 Sanriku-Oki earthquake, *Geophys. Res. Lett.*, *23*, 33–36.

Schwartz, S. Y., and J. M. Rokosky (2007), Slow slip events and seismic tremor at circum-Pacific subduction zones, *Rev. Geophys.*, *45*, RG3004, doi:10.1029/2006RG000208.

Sekine, S., and K. Obara (2006), A short-term slow slip event with deep low-frequency tremors at western part of Shikoku (April, 2006), *Rep. Coord. Comm. Earthquake Predict.*, *76*, 555–556.

Shelly, D. R., G. C. Beroza, S. Ide, and S. Nakamula (2006), Low-frequency earthquakes in Shikoku, Japan, and their relationship to episodic tremor and slip, *Nature*, *442*, 188–191.

Shelly, D. R., G. C. Beroza, and S. Ide (2007a), Non-volcanic tremor and low frequency earthquake swarms, *Nature*, *446*, 305–307.

Shelly, D. R., G. C. Beroza, and S. Ide (2007b), Complex evolution of transient slip derived from precise tremor locations in western Shikoku, Japan, *Geochem. Geophys. Geosyst.*, *8*, Q10014, doi:10.1029/2007GC001640.

S. Ide, Department of Earth and Planetary Science, University of Tokyo, 7-3-1 Hongo, Bunkyo, Tokyo, 113-0033, Japan. (ide@eps.s.u-tokyo.ac.jp)

K. Imanishi, National Institute of Advanced Industrial Science and Technology, Tsukuba Central 7, 1-1-1 Higashi, Tsukuba, Ibaraki, 305-8567, Japan. (imani@ni.aist.go.jp)

Y. Yoshida, Meteorological Research Institute, 1-1 Nagamine, Tsukuba, Ibaraki, 305-0052, Japan. (yyoshida@mri-jma.go.jp)

G. C. Beroza, Department of Geophysics, Stanford University, 397 Panama Mall, Stanford, CA 94305-2215, USA. (beroza@pangea.stanford.edu)

D. R. Shelly, Department of Earth and Planetary Science, University of California, 307 McCone Hall, Berkeley, CA 94720-4767, USA. (dshelly@seismo.berkeley.edu)